Analysis of Persistence in the Flood Timing and the Role of Catchment Wetness on Flood Generation in a Large River Basin in India

Yamini Rama Nandamuri, Poulomi Ganguli, Chandranath Chatterjee*

Department of Agricultural and Food Engineering, Indian Institute of Technology Kharagpur, West Bengal 721 302, India

**Correspondence to*: Dr. Poulomi Ganguli (pganguli@agfe.iitkgp.ac.in)

Abstract

This study contributes to the understanding of the timing of occurrence of floods and role of the catchment wetness in flood processes (i.e., magnitude and the timing of floods) over one of the largest tropical pluvial river basin system, Mahanadi, in India. Being located in the monsoon 'core' region (18° - 28° N latitude and 73° - 82° E longitude) and its proximity to Bay of Bengal, Mahanadi River Basin (MRB) system is vulnerable to tropical depression-induced severe storms and extreme precipitation-induced fluvial floods during southwest monsoon. Here we examine the incidence of flooding over MRB in recent decades (2007-2016) using monsoonal maxima peak discharge (MMPD) and peak over threshold (POT) events at 12 stream gauges, spatially distributed over the basin. We find the mean dates of flood occurrences are temporally clustered in the month of August for all gauges irrespective of the type of flood series. Our results reveal, sensitiveness of runoff responses (Flood Magnitude, FM and the Flood Timing, FT) to lagged *d-day* mean catchment wetness [CW] and corresponding catchment properties. Although we identify moderate to strong positive correlation between CW and flood properties at various lags, for the MMPD events, the nature of association between CW and FM, ranges between negative to modestly positive for the catchments with fine-textured soil, whereas catchments with medium textured soil showed moderately positive correlations. Further, we find FT is more strongly correlated (as manifested by statistically significant correlations) to CW rather than FM. Overall, we observe, the correlation of CW versus FT is negative, where the flood timing is relatively irregular. The outcomes of the study helps to improve predictability of floods, which can in turn enhance existing flood warning techniques.

Keywords: *Mahanadi River Basin, persistence, catchment wetness, flood magnitude, flood timing*

1. Introduction

Extreme events, such as floods affected more than 35 million people globally in 2018 (CRED, 2018). The frequent occurrence of floods globally has drawn attention to assess if the hydroclimatology of major river basins has changed (Pattanayak et al. 2017). According to National Commission on Floods, around 12% area of India (40 million ha) is flood prone, out of which the major flood prone areas are located in the eastern part of the country (FAO 2001; FAO 2015). Therefore, understanding dominant mechanisms behind flood generation processes is vital to take adaptive strategies, and can be useful for improving flood prediction and monitoring (Baldassarre et al. 2010; Xiao et al. 2013; Yang et al. 2014; Sakazume et al. 2016). The review of the literature suggest, physical factors, such as precipitation intensity, percentage of the impervious surface over the catchment, soil permeability, water holding capacity, topographic slopes, and the soil moisture content at the beginning of the storm event affect the severity of floods (Grillakis et al. 2016). However, out of all these factors, soil moisture is the only variable that can vary significantly on a daily to sub-daily time scales, and influences the partitioning of rainfall into evapotranspiration, infiltration, and runoff; hence plays a pivotal role in flood generation processes (Beck et al. 2009; Koster et al. 2010; Grillakis et al. 2016). Also in the framework of flood warning systems, soil moisture plays a pivot role (Georgakakos 2006; Javelle et al. 2010; Van Steenbergen and Willems 2013; Raynaud et al. 2015), due to the non-linear nature of runoff response to the rainfall (Zehe and Blöschl 2004; Hlavcova et al. 2005; Komma et al. 2007; Stephens et al. 2015).

Ye et al. (2017) examined the seasonality of annual maximum floods and the relative dominance of precipitation events and soil water storage in flood generation across the contiguous United States. The results revealed that the catchments where the antecedent soil water storage (storm rainfall) increased exhibited an increase (decrease) in flood seasonality. Merz et al. (2018) analyzed the role of catchment wetness and event precipitation on the spatial coherence of floods across Germany, and their findings indicated that significant spatial coherence was caused by persistence in catchment wetness rather than by persistent periods of higher/lower event precipitation. Many studies apart from mentioned above, concentrated on the role of antecedent soil moisture on peak flow discharge events (Grillakis et al. 2016; Saini et al. 2016; Sakazume et al. 2016; Vormoor et al. 2016; Blöschl et al. 2017). Chowdhury and Ward (2004) analyzed the effect of rainfall at the upstream catchments (India) on stream flows at downstream regions

(Bangladesh) in Ganges-Brahmaputra-Meghna Basins. Their findings suggested streamflows in Bangladesh are highly correlated with the rainfall in the upper catchments with typically a lag of about a month. Sharma et al. (2018) examined the changes in monthly streamflows and their linkages with rainfall variability in the Middle Tapi basin, India. It was observed that the trends in mean monthly streamflows were in phase with the trends in rainfall in respective sub-catchments.

The river Mahanadi, which is located in central-east (between 19°20' - 23°35'N latitudes and 80°30' - 86°50' E longitudes) part of the country (major source of freshwater for approximately 71 million people in the states of Chattisgarh and Odhisa) contributes to around 4.4% (1, 41, 589 km^2) of the total land mass with an average annual runoff of about 67 km^3 (NRSC-ISRO 2011, Pattanayak et al. 2017) is one of the largest peninsular rivers in India. Being located in the monsoon 'core' region (18° - 28° N latitude and 73° - 82° E longitude; Singh et al. 2014) and its proximity to the Bay of Bengal (adjacent to the north-west coast), the MRB is vulnerable to tropical depression-induced severe storms (Sahoo and Bhaskaran 2018) and monsoonal (June – September) extreme precipitation leading to severe floods. For example, recent consecutive flood events over MRB (2001, 2003, 2006, 2008, 2011, 2013, 2014 and 2016) have caused innumerable losses to economy and lives (NDMA 2019). Based on ground-based data from seven meteorological stations for the period 1901-80, Rao (1993) showed significant warming trend in mean maximum (up to 0.7°C per century) and average mean temperature (up to 0.5°C per century) during monsoon period over the basin. The warming trend over MRB (Rao 1993) was attributed to recent changes in land-use pattern, increase in population density and changes in agricultural practices over the region. Further, the recent increase in trends of the frequency and severity of high floods in MRB is linked to an increase in extreme rainfalls in the middle and the lower reaches of the basin (Panda et al. 2013; Jena et al. 2014). The review of the literature reveals, a number of studies (Rao and Kumar 1992; Rao 1993, 1995; Gosain et al. 2006; Mujumdar and Ghosh 2008; Ghosh et al. 2010; Mondal and Mujumdar 2012; Pattanayak et al. 2017) that analyzes detection and attribution of climate change signals over MRB.

Most of these earlier assessments were focused on changes in regional hydroclimatology as reflected in trends in precipitation, temperature and evapotranspiration (or changes in moisture regimes) patterns of observed (either station-based or gridded) meteorological records and projected (using large-scale general circulation models) climatic data over MRB. However, magnitude of fluvial peak discharge is typically modulated by both the storm rainfall and the catchment wetness prior to the storm event (Ettrick et al. 1987). Further, a review of literature suggests that heavy precipitation event (99^{th} percentile of daily precipitation) does not necessarily lead to peak discharge in streams (Ivancic and Shaw 2015; Wasko and Sharma 2017) since hydrologic response of the catchment is related to its antecedent moisture content, which is the most important contributing factor in modulating the nature of stream discharge. The urban (often smaller in area) catchments may have increased peak discharge, whereas the rural (often larger in size) catchments may experience decrease in runoff due to lower soil moisture content since high temperature may lead to drying up of soil more quickly in larger catchments leading to a large portion of precipitation not to become an overland flow. Nevertheless, storm runoff response could be highly sensitive to antecedent moisture content for smaller catchments as well (Dick et al. 1997).

Although a very few studies (Samantaray et al. 2019) investigate propagation of hydrological droughts over MRB considering the role of soil moisture deficit as an indicator of crop water stress, to the best of our knowledge no studies so far have investigated the link between catchment processes (such as catchment wetness) and extreme flood generating mechanisms over a large tropical river basin, such as MRB. To fill the gaps in the literature here we analyze the timing of floods over MRB in recent decades (post-2000s; from 2007 to 2016). The selection of time scale is motivated by the fact that floods over MRB is becoming more frequent in the recent past (Mahapatra 2015; Jena et al. 2014). To understand the effect of catchment wetness on flood properties (*i.e.*, severity and the timing of the event), following earlier studies (Ettrick et al. 1987; Ivancic and Shaw 2015) we select lagged *d*-day soil moisture data as an indicator for the catchment wetness over the sub-catchments of MRB. The soil moisture owing to its remarkable persistence (or memory) properties can influence the nature of runoff and its persistency (Koster et al. 2010; Orth and Seneviratne 2013). The outcomes of the study will be helpful in developing flood resiliency through nonstructural measures, such as improving predictability of floods for operational flood forecast models (Vivoni et al. 2006). Further, the modelling framework can be easily transferred to understand at which extent catchment-scale moisture content can influence the nature of flood properties in similar climatic regions as well as in the future climate projections.

The paper is organized as follows: the study region, dataset used and the modeling framework is described in Section 2. Section 3 presents the results and discussion. Finally, the salient conclusions of the study are presented in Section 4. The analyses are performed on entire MRB consisting of 12 stream gauge records. We select stream gauges based on least human interventions and the maximum data availability during the analyses period.

2. Data and methodology

2.1 Study Area

The river Mahanadi constitutes the sixth largest river basin in India with a drainage area of around 139681.51 km^2 (ArcGIS-based calculated area) and a total storage capacity of 14207.80 MCM (CWC, 2014). MRB is the lifeline of both Chattisgarh and Odisha states. As of the year 2013-14 estimates, Chattisgarh and Odisha together utilize around 13,715 MCM (~27.4%) and 2,074 MCM (~ 4%) of the river's water for irrigation and industrial purpose respectively (Dsouza et al. 2017b). We selected the entire MRB (80˚30' to 86˚50'E longitudes and 19˚20' to 23˚35'N latitudes) covering the states of Chhattisgarh (52.42%) and Odisha (47.14%) and small portions in Maharashtra (0.23%), Madhya Pradesh (0.11%) and Jharkhand (0.1%). Mahanadi River originates in Dhamtari district of Chhattisgarh and drains into the Bay of Bengal, spanning a total length of 851 km. The MRB is a rain-fed river with maximum precipitation observed between July and the first half of September in general and there is no significant contribution from groundwater recharge. December and January are the coldest months in the basin with the minimum temperature between 4˚C to 12˚C, and May is the hottest month with maximum temperature between 42˚C to 45˚C (CWC, 2014). Fig. 1 shows the spatial variability in elevation and stream gauge stations across the basin. The main soil types found in the basin are red and yellow soils, mixed red and black soils, laterite soils and deltaic soils. The basin has a culturable command area of about 7.99 M. ha as estimated in the 1990s, which is about 4% of the total cultivable area of the country (CWC, 2014).

2.2 Data Collection and Screening

The daily streamflow discharge data from 12 gauge stations (located between 81˚14' to 84˚45' E longitudes and 20˚05' to 23˚12' N latitudes) in the study area (Fig. 1) were obtained from the Central Water Commission (CWC), Government of India. All these stations have varying length of records; hence we have selected only those stations that have at least 70% data availability during monsoon months (June to September) with a minimum of 10 complete years of record. The catchment area of these stations varies between 950 and 11,960 km^2. Out of these 12 gauges, 11 are located in the Upper MRB (Region I, consists of total area of 84,700 km^2) and only one gauge, Kesinga, comprising the largest catchment area of 11,960 km^2 is located in the middle MRB (Region II, consists of total area of 50,745 km^2) [Fig. 1]. In the Delta region (i.e., lower MRB), the nature of flood flow is tidally influenced and prone to storm surges resulting into compound flooding from coastal storms and fluvial floods (OSDMA 2019), which leads to more complex flood mechanisms (Moftakhari et al. 2017). Hence, we exclude floods in the Delta region from the present analysis. Except the stream gauge at Manendragarh, which is located at around 293 km geodesic distance of Morga dam (an earthen dam of length 495 m; (NRSC-ISRO 2012)] all other gauges experience minimum human intervention. Nevertheless, Manendragarh area is amidst dense tropical deciduous forest with hilly and sandy soils and is the part of Northern Hills Agroclimatic zone of Chattisgarh state (Quamar and Bera 2017; Dsouza et al. 2017a). Further, it is located nearest to the source of MRB and at the highest elevation (~ 668 m above Mean Sea Level [MSL]) than that of the rest of the gauges. The MRB was delineated using the Shuttle Radar Topography Mission (SRTM) Digital Elevation Model of 90 m resolution (Jarvis et al. 2008) using Arc GIS10.1 software. The basin has the maximum and average elevations of 1319 m and 376.2 m above MSL respectively.

It is difficult to measure soil moisture on an in-situ basis at a catchment scale due to limited spatial and temporal availability of the soil moisture measurements (Grillakis et al. 2016; Seneviratne et al. 2006). On the other hand, the local soil moisture observations combined with simple analytical models (Albertson and Kiely 2001; Van den Dool et al. 2003) and/or the soil moisture data derived from the Land Surface Models (LSMs) have the caveat of the plausible model dependency of the obtained results (Seneviratne et al. 2006). Further, LSMs (for example, Variable Infiltration Capacity [VIC; Livneh et al. 2013]) may be better at handling surface and subsurface hydrological processes but may suffer from cascading uncertainty across various model components. An alternative is the retrieval of soil moisture data from satellite sensors such as the series of passive multi-frequency radiometers (SMMR, SSM/I, Windsat & SMOS, AMSR-E, etc.), active microwave scatterometers (ASCAT-A, AMI-WS, etc.) and combined soil moisture (Chung et al.

2018). The combined soil moisture estimates (Chung et al. 2018) are generated by blending passive and active microwave soil moisture retrieval algorithm. The surface soil moisture were obtained from the Essential Climate Variable-Soil Moisture (ECV-SM) data under the European Space Agency (ESA)-Climate Change Initiative (Liu et al. 2012; Dorigo et al. 2017; Gruber et al. 2017; Samantaray et al. 2019). The ECV-SM global soil moisture combined dataset (Chung et al. 2018) provides volumetric soil moisture (m^3/m^3) at daily time step and at 0.25° grid resolution from 1978 to 2018. However, in early years the spatial coverage of soil moisture data is lower because of limited number of available sensors.

2.3 Modelling Framework

We analyse the two methods of flood samplings, namely monsoonal (June-September) maxima peak discharge (MMPD) and Peak over Threshold (POT) events. Further, we characterize the timing of flood occurrences using circular statistics. We detect the correlations of catchment wetness (CW) versus flood magnitude (FM); and catchment wetness (CW) versus flood timing (FT) using Kendall's Tau statistics. In the subsequent sections, we have described each of these modeling components:

2.3.1 Extraction of Monsoonal Maximum Peak Discharge (MMPD) Events and Peak over Threshold (POT) Events

The most common indicator of flood trends in rain-fed basins in India is the monsoonal maximum discharge events (Rakhecha 2002), i.e., the largest daily mean streamflow during monsoon (June to September) months in each hydrologic year (1 June – 31 May). First, we selected the independent peak flows during monsoon season (one event per year) from daily mean streamflow records from all 12 gauges. A few studies (Svensson et al. 2005; Burn et al. 2016) have suggested that POT series gives more information about statistical attributes of extremes as compared to the MMPD, revealing a better temporal pattern of flood occurrence. On the other hand, selecting a suitable threshold value for extracting POT data is one of the challenging aspects (Burn et al. 2016). Hence, we checked various thresholds, ranging from 98 to 99.9^{th} percentiles at an interval of 0.5, and then finalized a threshold based on 98.5^{th} percentile to select on an average 3-peak discharge events per year. To guarantee independent POT events, based on catchment area (which is less than 45,000 km^2 for all gauges), we selected decluster time of 5 days (Svensson et al. 2005;

Petrow and Merz 2009) between events. If two or more consecutive POT events occurred within the specified period, the smaller events are dropped, and the highest event is chosen for the analysis.

2.3.2 Detection of Flood Timing and its Persistence of peak discharge events

We detect the flood timing or the time (or date) of occurrence of the event using the directional or circular statistics (Mardia 1972; Pewsey et al. 2013; Tian et al. 2011; Dhakal et al. 2015; Burn et al. 2016). Laaha and Blöschl (2006) summarized the flood seasonality indices and how they can be estimated based on the peak discharge time series. In this method, the date of occurrence of a peak flow, as a directional statistic of time, is translated into location on the circumference of a circle, with the mathematical convention that the start of the flood season is shown at its most easterly point and time proceeds in a counter-clockwise direction (Mardia 1972; Fisher 1993). Once individual dates of flood occurrences are expressed as a directional variable, then directional mean and variance can be calculated.

The date of flood occurrence *(Julian Date)*$_i$ can be converted to an angular value (θ_i), in radians for an event "*i*" using:

$$\theta_i = (Julian\,Date)_i \frac{2\pi}{len(yr)} \tag{1}$$

Where, *Julian Date* = 1 for 1 January and *Julian Date* = 365 for 31 December (or 366 for leap year); *len* (*yr*) is the number of days in a year, i.e., 365 for a normal year and 366 for a leap year. For a sample of *n* events, the X - and Y -coordinates of the mean date can be determined as (Burn and Whitfield 2018)

$$\bar{X} = \frac{\sum_{i=1}^{n} q_i \cos\theta_i}{\sum_{i=1}^{n} q_i}; \bar{Y} = \frac{\sum_{i=1}^{n} q_i \sin\theta_i}{\sum_{i=1}^{n} q_i} \tag{2}$$

Here, the equation (2) is derived using the weighted average of extreme events by weighing the peak discharge. Here, $\overline{X}$ and $\overline{Y}$ represent the x- and y-coordinates of the mean event date. Based on the time of occurrence of a flood event in a year, the mean event angle is obtained by

$$Mean\ Angle = \begin{cases} \tan^{-1}\left(\frac{\overline{Y}}{\overline{X}}\right), & if\ \overline{X} > 0\ and\ \overline{Y} > 0 \\ 180 - \tan^{-1}\left(\frac{\overline{Y}}{\overline{X}}\right), & if\ \overline{X} < 0\ and\ \overline{Y} > 0 \\ 180 + \tan^{-1}\left(\frac{\overline{Y}}{\overline{X}}\right), & if\ \overline{X} < 0\ and\ \overline{Y} < 0 \\ 360 - \tan^{-1}\left(\frac{\overline{Y}}{\overline{X}}\right), & if\ \overline{X} > 0\ and\ \overline{Y} < 0 \end{cases} \quad (3)$$

The mean event date (*MD*) can then be determined as:

$$MD = Mean\ Angle \times \left(\frac{len\ yr}{2\pi}\right) \quad (4)$$

The persistence ($\overline{r}$) of extreme events can be determined from:

$$\overline{r} = \sqrt{\overline{X}^2 + \overline{Y}^2}, \quad 0 \le \overline{r} \le 1 \quad (5)$$

The dimensionless statistic '*r*' indicates the variability in the timing of flood events with $\overline{r}$ = 0, indicates no persistence, i.e., flood events are uniformly distributed throughout the year, whereas, $\overline{r}$ = 1 indicates high persistence, i.e., all floods at a station occur on the same day of the year (Laaha and Blöschl 2006). Mean date of flood occurrence may occur at a period of the year when no events are observed (Burn and Whitfield 2018). Circular variance provides the variability of peak discharge events about the mean date for individual stations (Dhakal et al. 2015). The long-term evolution of the circular variance σ^2 is computed using the expression:

$$\sigma^2 = -2\ln(\bar{r}) \tag{6}$$

2.3.3 Extraction of Mean Catchment Wetness

Assessing the role of catchment wetness on the timing of flood occurrences provides useful insights regarding the nature of flood seasonality in the future climate (Ye et al. 2017). A few studies (Berghuijs et al. 2016) reported that soil water storage before floods correlated more strongly with floods than daily rainfall. While previous studies (Rao and Kumar 1992; Rao 1993, 1995; Panda et al. 2013; Jena et al. 2014) have focused on role of atmospheric drivers, such as precipitation and temperature in modulating nature of streamflow, here we explore the potential linkage of soil moisture memory in flood generating mechanisms.

As we were interested in monsoonal months, gridded soil moisture data in between 15th May and 31st October (during mid of summer to fall) for each year were extracted over entire MRB. Mean areal CW over individual catchments for each year was calculated using area-weighted mean soil moisture values; where the total weight of a grid was computed as the cosine of the latitude of the grid multiplied by the fraction of catchment area lying in the individual grid location (Ganguli et al. 2017). For many of the catchments over MRB, the soil moisture data was missing, so we selected only those catchments, which have at least 40% data availability during monsoon to fall season (15th May to 31st October) for each year. The choice of season is based on the timing of floods over MRB since extreme precipitation is one of the primary flood generating mechanisms over the basin. Finally, 12 catchments were selected with data varying from 2007 to 2016 (10 years length; the catchment-wide soil moisture data before 2006 were unavailable). Gaps in the weighted mean soil moisture time series at individual catchments were infilled using time series interpolation technique with a shape-preserving piecewise cubic polynomial function, which is one of the commonly used methods to estimate missing records in hydrology (Mizumura 1985; Price et al. 2000). Unlike other interpolants (such as linear and spline), this interpolation function can preserve local monotonic trends in the dataset such that the extreme artifacts are not introduced in the unfilled data set (Ganguli and Ganguly 2016).

2.3.4 Correlation analysis using Kendall's Tau

Several studies in the past reported that antecedent soil moisture states could be one of the primary governing factors in modulating the timing and intensity of floods (Seneviratne et al. 2006; Merz and Blöschl 2009; Norbiato et al. 2009; Marchi et al. 2010; Orth and Seneviratne 2013; Berghuijs et al. 2016; Ye et al. 2017). We used the mean CW values at each of the sites at most 40 days prior and at least ten days later (*i.e.*, time lags of d = -40, -30, -29, …., -1, 0, +1, 2, …, 10 days, comprising a total of 51 days record including the flood event day) to each MMPD and POT events to investigate the association between CW and flood properties (i.e., FM and FT). This is to understand the influence of catchment-scale soil moisture memory at different time lags on runoff responses. Flood timings of individual flood events are taken as an angular value obtained from the Eq. 1 for both MMPD and POT events. The strength of dependency of CW versus flood properties was measured using a rank-based nonparametric correlation measure Kendall's tau (τ). It measures the strength of monotonic relationship between two continuous random variables including the nonlinear associations and is robust to outliers (unlike Pearson's product moment correlation coefficient, r) present in the data.

The population version of the Kendall's τ rank correlation coefficient is defined as the difference between the probability of concordance and the probability of discordance. Given, two variables X and Y, sampled jointly from a bivariate distribution, the test statistic S is calculated by subtracting the number of "discordant pairs" M [i.e., the number of (x,y) pairs where y decreases as x increases], from the number of "concordant pairs" P [i.e., the number of (x,y) pairs where y increases with increasing x]:

$$S = P - M \tag{7}$$

Where, P = "number of pluses", the number of times the y's increase as the x's increase, or the number of $y_i < y_j$ for all $i < j$,

M = "number of minuses," the number of times the y's decrease as the x's increase, or the number of $y_i > y_j$ for $i < j$

for all $i = 1,....(n - 1)$ and $j = (i+1), ... n$

Kendall's tau correlation coefficient is given by (Helsel and Hirsch 2002)

$$\tau = \frac{S}{n(n-1)/2} \tag{8}$$

On the other hand, another rank correlation statistic, Spearman's Rho, which is estimated by the correlation coefficient of the corresponding rank of the two variables, is not as interpretable as a difference between probabilities (Newson 2002). Typically, Tau values are lower than values of the traditional correlation coefficient, *r* for a linear association of the same strength because of different scale of correlation. Kendall's tau value lies between -1 and 1; where positive (negative) values indicate perfect positive (negative) association between two variables.

3. Results and Discussion

3.1 Timing of Flood Occurrence and its Persistence

Analyzing the variability in the timing of floods from year to year is crucial for the efficient water resources management and understanding space-time variability of floods in a changing climate (Ye et al. 2017). The dates of flood occurrence for both MMPD and POT discharge events are converted to an angular value using Eq. 1 and are plotted in a polar plot as shown in Fig. 2. The occurrence date of flood for each of the stations is represented as an angle measured counterclockwise relative to 1st January, and the mean catchment elevations of stream gauges are shown as the distance from the center of the polar plot. For MMPD events, the floods varied from June ending to September; since it is one extreme event per year, all the extremes were observed within the monsoonal period (June to September). But for POT events, it includes more than one extreme event per year; hence few floods are observed in the month of October as well.

The seasonality in flood responses is determined using directional statistics. The changes in the timing (mean date), flood variability (σ) and persistence $(\bar{r})$ are evaluated for individual stream gauge locations. Seasonality measures of MMPD and POT peak discharge events are plotted in a polar plot as shown in Fig. 3. The mean occurrence date of flood for each of the stations is represented as an angle measured counterclockwise relative to 1st January, and the persistence of the flood events are shown as the distance from the center of the polar plot. For both MMPD and

POT peak discharge events, the seasonality analysis indicates the persistence of floods across all gauges with mean flood dates occurring in the month of August. Kotni gauge station, situated at the Upper MRB (Region I), showed the mean flood date at 1st and 2nd of August for MMPD (Fig. 3; *left panel*) and POT events (Fig. 3; *right panel*) respectively. On the other hand, Ghatora and Paramanpur gauge stations showed the mean flood date at 28th and 29th of August (close to September) for MMPD (Fig. 3; *left panel*) and POT events (Fig. 3; *right panel*) respectively. Among individual stream gauge stations, POT events showed persistence in the range of 0.88-0.95 while MMPD events showed persistence in the range of 0.86-0.98. Likewise, we observe the largest circular variance for the site Rampur and the least for the site Kelo for the MMPD events. For POT events, the largest circular variance was observed for the site Sundargarh and the least for the site Ghatora respectively. However, taken together, we infer that the peak discharge events are highly persistent throughout MRB. Our results are in agreement with Burn and Whitfield (2018), in which authors found that stream gauges in the pluvial flood regime, in general, show a very few (significant) changes in flood seasonality than that of the other flood regimes. Fig. 4 presents the spatial map of persistence in flood timing for both MMPD and POT events, which suggest larger spatial variability in flood timing for MMPD events than that of the POT events. This can provide useful information for water management perspectives, especially for the large river basin, such as MRB.

3.2 Role of Catchment Wetness in Flood Generation

It is critical to understand the role of specific hydrometeorological drivers that lead to extreme floods; which is an important step towards assessing the predictability of floods, especially in an era of human-induced climate change (Mora et al. 2017; Yin et al. 2018; Best 2019). To discern the association of CW versus flood characteristics (i.e., flood magnitude and timing), we analyze the lagged daily CW at least 40-days prior and at most 10-days later to the date of occurrence of the extreme flood event. The association was determined using rank-based Kendall's τ statistics between weighted mean CW at individual catchment and the flood characteristics. The resulting correlation values are visualized using the heat map. Figs. 5 - 6 present a measure of association between the CW and FM followed by the CW and FT for both MMPD and POT events.

First, in Fig. 5, catchment characteristics, such as soil texture and topography played a key role in detecting the nature of correlation between CW and FM. A study on an experimental catchment by Nasta et al. (2013) suggested that spatial soil moisture distribution depends on catchment topography during wet periods whereas, during dry periods, it depends primarily on soil hydraulic properties. The fine textured soil with moderate to gently sloping catchments [Figs. 6 and 8 in Central Water Commission Technical Report, CWC (2014)], in general, showed modest to negative correlation, while the medium textured soil with level land surface catchments showed moderate to strong positive association with floods. Even though Manendragarh catchment has medium textured soil, it has gently sloping land surface (which drains the water); that may cause a negative correlation between CW versus FM for both MMPD and POT events. Further, as pointed above, an earthen dam is located near this site. Likewise, for MMPD events, Baronda catchment has medium textured soil and level to gentle slope surface leading to a strong correlation just three days before the date of flooding. Pathardhi has mostly fine textured soil type and level topography leading to a modest correlation value up to 20-days before the date of flooding for the MMPD event, whereas, no sign of association was observed for the POT event. For POT events, low elevation areas showed modest to negative correlation from the date of flooding to 40 days prior to the flood event.

Second, in Fig. 6 (the heat map of correlation between CW and FT), we find moderate to strong positive correlations for lags 1 to 40 days for most of the gauges, with stronger positive correlation values for the MMPD events than that of the POT events. However, the catchments, Sundargarh and Kesinga showed negative correlations at a few instances due to less persistence in flood timings relative to other gauges. Our findings corroborate well with Ye et al. (2017), in which the authors identified catchments with high moisture storage showed high persistence in flood timing, whereas the catchments associated with low antecedent moisture storage are associated with low persistence in the flood timing. Overall, our results indicate that FT is more strongly correlated to CW rather than FM.

Finally, we present a spatial map (Fig. 7) showing maximum Kendall's tau value out of 51 days record including the date of the flood event for each station for both method of flood sampling. This map is informative for water resources managers and stakeholders for flood predictability studies over the basin, especially for developing an early warning system. For the MMPD events (Fig. 7; *left panel*), Manendragarh, Kotni, and Kesinga catchments showed the maximum correlation values (FM versus CW) in the range of 30 to 40 days prior to the flood event date while Kurubhata and Kelo catchments showed maximum correlation on the day of flooding. In contrast, unlike MMPD events, for the POT events (Fig. 7; *right panel*), none of the catchments show the maximum correlation with flood magnitude on the day of flooding. Likewise, we present spatial maps for CW and FT for both MMPD and POT (Fig. 8). For the MMPD events (Fig. 8 (*left panel*)), half of the catchments showed the highest correlation between 30 and 40 days prior to the flood event date, while for POT events (Fig. 8 (*right panel*)) most of the catchments (66.6%) showed the highest correlation on the 40^{th} day prior to the date of flooding.

Tables 1 - 2 show highest correlation (maximum Kendall's tau) values of mean CW versus FM, and mean CW versus FT for each of the sites, corresponding time-lags (in days) along with their catchment area respectively. Here, we note that for smaller catchments (< 1000 km^2 for example, Kelo with catchment area 950 km^2) the severe flood can happen at zero to one day time lag (Table 1). This is in agreement with earlier studies (Ivancic and Shaw 2015; Wasko and Sharma 2017) in which authors have inferred that unlike larger catchments, the smaller catchment may have an early occurrence of increased peak discharge. On the other hand, we could not find any specific trend between catchment area and the time lags for the timing of the flood event (Table 2).

4. Summary and Conclusions

This paper contributes to the assessment of the relation between catchment wetness and flood processes in the Mahanadi river basin. Unlike previous assessments (Panda et al. 2013; Jena et al. 2014), here we investigate two novel aspects: *first*, we assess the persistence of the flood events, in the recent decades (from 2007 – 2016) using directional statistics. Second, we evaluate the role of catchment wetness (CW) in modulating the flood flow processes using a rank-based correlation statistic. While most of the earlier assessments are limited to analyzing sensitiveness of hydrometeorological forcing, precipitation to peak discharge generation at MRB, to the best of our knowledge, this study is the first to investigate the linkage between flood generation and catchment wetness, and evaluate the extent to which soil moisture memory (at different time lags) may influence the severity and the timing of the flood event in a large river basin in a tropical environment.

The key insights from the study are summarized as follows:

- The seasonality of flood responses in both methods of flood samplings suggests the mean dates of flood occurrences are temporally clustered in the month of August. The MMPD events showed more variability in the persistence in flood timing than that of the POT events. Finally, our study suggests the peak discharge events are highly persistent over the past decade.

- Our results reveal sensitiveness of runoff (both magnitude and the time of occurrence) to lagged *d-day* soil moisture content (an indicator of CW) and corresponding soil properties. For the MMPD events, the nature of association between CW and FM ranges between negative to near zero for the fine-textured soil, whereas the catchment with medium textured soil showed the positive correlations. Further, we find FT is more strongly correlated to CW rather than FM. The correlation between CW and FT tend to become negative in catchments with relatively less persistent nature of the timing of the flood peak.

A few caveats could be considered. The specific insights presented here are conditioned on the quality of site-specific information used in the analyses. Based on the availability of good quality records, the analysis is limited to the recent ten years. It is nonetheless interesting to evaluate the role of catchment processes utilizing recently released high-resolution soil moisture records (Nayak et al. 2018), which is available at 4 km spatial resolution over the past 14-years (2001-2014) period. Finally, it would be interesting to investigate the uncertainty among different dataset (i.e., data derived from various sources) in flood generation processes (Vivoni et al. 2006; Amengual et al. 2008) in a large river basin, such as MRB.

Acknowledgments

The authors sincerely thank the Department of Science and Technology (DST), Government of India, for financial support. This study was organized as a part of the Center of Excellence (CoE) in Climate Change studies activity established at IIT Kharagpur and funded by DST, Government of India. This study forms a part of the sub-project “Impact of Climate Change on Flood Risk” conducted under the CoE in Climate Change at IIT Kharagpur. We are also thankful to the Central Water Commission (CWC), Government of India, for providing the data sets for this research. We especially thank the European Space Agency (ESA)-Climate Change Initiative for their support in data extraction. We are thankful to Philip Buttinger, TU Wien, for clarifying technical queries pertaining to ECV-SM global soil moisture combined data product.

References

Albertson JD, Kiely G (2001) On the structure of soil moisture time series in the context of land surface models. J Hydrol 243:101–119

Amengual A, Romero R, Alonso S (2008) Hydrometeorological ensemble simulations of flood events over a small basin of Majorca Island, Spain. Q J R Meteorol Soc 134:1221–1242

Baldassarre G Di, Montanari A, Lins H, et al. (2010) Flood fatalities in Africa : from diagnosis to mitigation. Geophys Res Lett 37:1–5

Beck HE, De JR, Schellekens J, et al. (2009) Improving Curve Number Based Storm Runoff Estimates Using Soil Moisture Proxies. IEEE J Sel Top Appl EARTH Obs Remote Sens 2:250–259

Berghuijs WR, Woods RA, Hutton CJ, Sivapalan M (2016) Dominant flood generating mechanisms across the United States. Geophys Res Lett 43:4382–4390

Best J (2019) Anthropogenic stresses on the world’s big rivers. Nat Geosci 12:7–21

Blöschl G, Hall J, Parajka J, et al. (2017) Changing climate shifts timing of European floods. Science 357:588–590

Burn DH, Whitfield PH (2018) Changes in flood events inferred from centennial length streamflow data records. Adv Water Resour 121:333–349

Burn DH, Whitfield PH, Sharif M (2016) Identification of changes in floods and flood regimes in Canada using a peak over threshold approach. Hydrol Process 30:3303–3314

CRED (Centre for Research on the Epidemiology of Disasters) (2018) Review of Disaster Events. Université catholique de Louvain, Belgium. https://www.cred.be/. Accessed April 2019

CWC (Central Water Commission) (2014) Mahanadi Basin. CWC and NRSC, New Delhi pp 110

Chowdhury MR, Ward N (2004) Hydro-meteorological variability in the greater Ganges-Brahmaputra-Meghna basins. Int J Climatol 24:1495–1508

Chung D, Dorigo W, De Jeu R, et al. (2018) ESA Climate Change Initiative Phase II - Soil Moisture. Product Specification Document (PSD) D1.2.1 Version 4.2. pp 1-50

Dick GS, Anderson RS, Sampson DE (1997) Controls on flash flood magnitude and hydrograph shape, Upper Blue Hills badlands, Utah. Geology 25:45–48

Dhakal N, Jain S, Gray A, et al. (2015) Nonstationarity in seasonality of extreme precipitation: A nonparametric circular statistical approach and its application. Water Resour Res 51:4499–4515

Dsouza CJ, Joy KJ, Bhadbhade N, et al (2017a) Mahanadi River Basin: A Situation Analysis. Forum for Policy Dialogue on Water Conflicts in India pp 1–78

Dsouza C, Samuel A, Bhagat S, Joy KJ (2017b) Water Allocations and Use in the Mahanadi River Basin - A Study of the Agricultural and Industrial Sectors. Forum for Policy Dialogue on Water Conflicts in India pp 1–168

Dorigo W, Wagner W, Albergel C, et al. (2017) ESA CCI Soil Moisture for improved Earth system understanding: State-of-the-art and future directions. Remote Sens Environ 203:185–215

Ettrick TM, Mawdlsey JA, Metcalfe AV (1987) The influence of antecedent catchment conditions on seasonal flood risk. Water Resour Res 23:481–488

FAO (Food and Agriculture Organization of the United Nations) (2001) Report of the FAO Asia-Pacific Conference on Early Warning, Prevention, Preparedness and Management of Disasters in Food and Agriculture. Food and Agricultural Organization of United Nations. http://www.fao.org/3/AC120E/AC120e00.htm. Accessed April 2019

FAO (Food and Agriculture Organization of the United Nations) (2015) Aquastat Report: India. Food and Agricultural Organization of United Nations. http://www.fao.org/aquastat/en/. Accessed April 2019

Fisher NI, Lewis T, Embleton BJJ (1993) Statistical analysis of spherical data. Cambridge university press pp 329

Ganguli P, Ganguly AR (2016) Space-time Trends in U. S. Meteorological Droughts. J. Hydrol.: Regional Studies 8:235–259

Ganguli P, Kumar D, Ganguly AR (2017) US Power Production at Risk from Water Stress in a Changing Climate. Sci Rep 7:11983

Ghosh S, Raje D, Mujumdar PP (2010) Mahanadi streamflow: climate change impact assessment and adaptive strategies. Curr Sci 98:1084–1091

Gosain AK, Rao S, Basuray D (2006) Climate change impact assessment on hydrology of Indian river basins. Curr Sci 90:346–353

Georgakakos KP (2006) Analytical results for operational flash flood guidance. J Hydrol 317:81–103

Grillakis MG, Koutroulis AG, Komma J, et al. (2016) Initial soil moisture effects on flash flood generation – A comparison between basins of contrasting hydro-climatic conditions. J Hydrol 541:206–217

Gruber A, Dorigo WA, Crow W, Wagner W (2017) Triple Collocation-Based Merging of Satellite Soil Moisture Retrievals. IEEE Trans Geosci Remote Sens 55:6780–6792

Helsel DR, Hirsch RM (2002) Statistical Methods in Water Resources Techniques of Water Resources Investigations. U.S. Geological Survey, Book 4, chapter A3, pp 522

Hlavcova H, Kohnova S, Kubes R, et al. (2005) An empirical method for estimating future flood risks for flood warnings. Hydrol. Earth Syst. Sci. 9: 431-448

Ivancic TJ, Shaw SB (2015) Examining why trends in very heavy precipitation should not be mistaken for trends in very high river discharge. Clim Change 133:681–693

Jarvis A, Reuter HI, Nelson A, Guevara, E (2008) Hole-filled SRTM for the globe Version 4, available from the CGIAR-CSI SRTM 90m Database. CGIAR CSI Consort Spat Inf 1–9. doi: 10.1167/iovs.10-6319

Javelle P, Fouchier C, Arnaud P, Lavabre J (2010) Flash flood warning at ungauged locations using radar rainfall and antecedent soil moisture estimations. J Hydrol 394:267–274

Jena PP, Chatterjee C, Pradhan G, Mishra A (2014) Are recent frequent high floods in Mahanadi basin in eastern India due to increase in extreme rainfalls? J Hydrol 517:847–862

Komma J, Reszler C, Blöschl G, Haiden T (2007) Ensemble prediction of floods? catchment non-linearity and forecast probabilities. Nat. Hazards Earth Syst. Sci. 7:431-444

Koster RD, Mahanama SPP, Livneh B, et al. (2010) Skill in streamflow forecasts derived from large-scale estimates of soil moisture and snow. Nat Geosci 3:613–616

Laaha G, Blöschl G (2006) Seasonality indices for regionalizing low flows. Hydrol Process 20:3851–3878

Liu YY, Dorigo WA, Parinussa RM, et al. (2012) Trend-preserving blending of passive and active microwave soil moisture retrievals. Remote Sens Environ 123:280–297

Livneh B, Rosenberg EA, Lin C, et al (2013) A Long-Term Hydrologically Based Dataset of Land Surface Fluxes and States for the Conterminous United States: Update and Extensions. J Clim 26:9384–9392

Mahapatra, R. (2006). Disaster dossier: The impact of climate change on Orissa. Infochange Environ pp 9

Marchi L, Borga M, Preciso E, Gaume E (2010) Characterisation of selected extreme flash floods in Europe and implications for flood risk management. J Hydrol 394:118–133

Mardia KV. (1972) Statistics of directional data. Academic Press. https://www.elsevier.com/books/statistics-of-directional-data/mardia/978-0-12-471150-1. Accessed October 2018

Merz B, Dung NV, Apel H, et al. (2018) Spatial coherence of flood-rich and flood-poor periods across Germany. J Hydrol 559:813–826

Merz R, Blöschl G (2009) Process controls on the statistical flood moments - a data based analysis. Hydrol Process 23:675–696

Mizumura K (1985) Estimation of Hydraulic Data by Spline Functions. J Hydraul Eng 111:1219–1225

Mora C, Dousset B, Caldwell IR, et al. (2017) Global risk of deadly heat. Nat Clim Chang 7:501–506

Moftakhari HR, Salvadori G, AghaKouchak A, et al (2017) Compounding effects of sea level rise and fluvial flooding. Proc Natl Acad Sci 114:9785–9790

Mondal A, Mujumdar PP (2012) On the basin-scale detection and attribution of human-induced climate change in monsoon precipitation and streamflow. Water Resour Res 48:1–18

Mujumdar PP, Ghosh S (2008) Modeling GCM and scenario uncertainty using a possibilistic approach: Application to the Mahanadi River, India. Water Resour Res 44: 1–15

NDMA (National Disaster Management Authority) (2019) Major disasters in India. https://ndma.gov.in/en/disaster-data-statistics.html. Accessed April 2019

Nasta P, Sica B, Chirico G., et al. (2013) Analysis of Near-surface Soil Moisture Spatial and Temporal Dynamics in an Experimental Catchment in Southern Italy. Procedia Environ Sci 19:188–197

Newson R (2002) Parameters behind "nonparametric" statistics: Kendall's tau, Somers' D and median differences. Stata J 2:45–64

NRSC-ISRO (2011) Surface water resources. India-WRIS, Jodhpur. http://india-wris.nrsc.gov.in/wrpinfo/index.php?title=Surface_water_resources. Accessed April 2019

NRSC-ISRO (2012) Morga Dam D00376. India-WRIS, Jodhpur. http://india-wris.nrsc.gov.in/wrpinfo/index.php?title=Morga_Dam_D00376. Accessed April 2019

Nayak HP, Osuri KK, Sinha P, et al. (2018) High-resolution gridded soil moisture and soil temperature datasets for the indian monsoon region. Sci Data 5:180264

Norbiato D, Borga M, Merz R, et al (2009) Controls on event runoff coefficients in the eastern Italian Alps. J Hydrol 375:312–325

Orth R, Seneviratne SI (2013) Propagation of soil moisture memory to streamflow and evapotranspiration in Europe. Hydrol Earth Syst Sci 17:3895–3911

OSDMA (Odisha State Disaster Management Authority) (2019) Floods is Orissa. http://www.osdma.org/ViewDetails.aspx?vchglinkid=GL002&vchplinkid=PL006. Accessed April 2019

Panda DK, Kumar A, Ghosh S, Mohanty RK (2013) Streamflow trends in the mahanadi river basin (India): Linkages to tropical climate variability. J Hydrol 495:135–149

Pattanayak S, Nanjundiah RS, Kumar DN (2017) Linkage between global sea surface temperature and hydroclimatology of a major river basin of India before and after 1980. Environ Res

Lett 12:124002

Petrow T, Merz B (2009) Trends in flood magnitude, frequency and seasonality in Germany in the period 1951-2002. J Hydrol 371:129–141

Pewsey A, Neuhäuser M, Ruxton GD (2013) Circular Statistics in R. Oxford University Press pp 182

Price DT, McKenney DW, Nalder IA, et al. (2000) A comparison of two statistical methods for spatial interpolation of Canadian monthly mean climate data. Agric For Meteorol 101:81–94

Quamar MF, Bera SK (2017) Pollen analysis of modern tree bark samples from the Manendragarh Forest Range of the Koriya district, Chhattisgarh, India. Grana 56:137–146

Rakhecha PR (2002) Highest floods in India. The Extremes of the Extremes: Extraordinary Floods (Proceedings of a symposia held at Reykjavik, Iceland, July 2000), IAHS Publ. no. 271

Rao PG (1993) Climatic changes and trends over a major river basin in India. Clim Res 2:215–223

Rao PG (1995) Effect of climate change on streamflows in the Mahanadi River Basin, India. Water Int 20:205–212

Rao PG, Kumar KK (1992) Climatic shifts over Mahanadi river basin. Curr Sci 63:192–196

Raynaud D, Thielen J, Salamon P, et al. (2015) A dynamic runoff co-efficient to improve flash flood early warning in Europe: Evaluation on the 2013 central European floods in Germany. Meteorol Appl 22:410–418

Sahoo B, Bhaskaran PK (2018) Multi-hazard risk assessment of coastal vulnerability from tropical cyclones – A GIS based approach for the Odisha coast. J Environ Manage 206:1166–1178

Saini R, Wang G, Pal JS (2016) Role of Soil Moisture Feedback in the Development of Extreme Summer Drought and Flood in the United States. J Hydrometeorol 17:2191–2207

Sakazume R, Ryo M, Saavedra O (2015) Consideration of Antecedent Soil Moisture for Predicting Flood Characteristics. J Japan Soc Civ Eng Ser B1 (Hydraulic Eng) 71:I_97-I_102

Samantaray AK, Singh G, Ramadas M, Panda RK (2019) Drought hotspot analysis and risk assessment using probabilistic drought monitoring and severity–duration–frequency analysis. Hydrol Process 33:432–449

Seneviratne SI, Koster RD, Guo Z, et al (2006) Soil Moisture Memory in AGCM Simulations: Analysis of Global Land–Atmosphere Coupling Experiment (GLACE) Data. J Hydrometeorol 7:1090–1112

Singh D, Tsiang M, Rajaratnam B, Diffenbaugh NS (2014) Observed changes in extreme wet and dry spells during the South Asian summer monsoon season. Nat Clim Change 4:456–461

Sharma PJ, Patel PL, Jothiprakash V (2018) Changes in monthly hydro-climatic indices for middle Tapi basin, India pp 1-14

Stephens E, Day JJ, Pappenberger F, Cloke H (2015) Precipitation and floodiness. Geophys Res Lett 42:10316–10323

Svensson C, Kundzewicz WZ, Maurer T (2005) Trend detection in river flow series: 2. Flood and low-flow index series. Hydrol Sci J 50:811–824

Tian P, Zhao GJ, Li J, Tian K (2011) Extreme value analysis of streamflow time series in Poyang Lake Basin, China. Water Sci Eng 4:121–132

Van Steenbergen N, Willems P (2013) Increasing river flood preparedness by real-time warning based on wetness state conditions. J Hydrol 489:227–237

Van den Dool H, Huang J, Fan Y (2003) Performance and analysis of the constructed analogue method applied to US soil moisture over 1981–2001. J Geophys Res Atmospheres 108, D16, 8617

Vivoni ER, Entekhabi D, Bras RL, et al. (2006) Extending the Predictability of Hydrometeorological Flood Events Using Radar Rainfall Nowcasting. J Hydrometeorol 7:660–677

Vormoor K, Lawrence D, Schlichting L, et al. (2016) Evidence for changes in the magnitude and frequency of observed rainfall vs. snowmelt driven floods in Norway. J Hydrol 538:33–48

Wasko C, Sharma A (2017) Global assessment of flood and storm extremes with increased temperatures. Sci Rep 7:1–8

Xiao Y, Wan J, Hewings GJD (2013) Flooding and the Midwest economy : assessing the Midwest floods of 1993 and 2008. GeoJournal 78:245–258

Yang L, Tian F, Smith JA, Hu H (2014) Urban signatures in the spatial clustering of summer heavy rainfall events over the Beijing metropolitan region. Journal of Geophysical Research : Atmospheres. J Geophys Res Atmos 119:1203–1217

Ye S, Li H-Y, Leung LR, et al. (2017) Understanding Flood Seasonality and Its Temporal Shifts within the Contiguous United States. J Hydrometeorol 18:1997–2009

Yin J, Gentine P, Zhou S, et al. (2018) Large increase in global storm runoff extremes driven by climate and anthropogenic changes. Nat Commun 9:4389

Zehe E, Blöschl G (2004) Predictability of hydrologic response at the plot and catchment scales: Role of initial conditions. Water Resour Res 40:1–21

Table 1 Catchment-wise highest lagged *d*-day (varies from zero, the date of flood occurrence to 40 days prior to the event) correlation value of CW versus FM. The correlation values are computed using rank-based Kendall's tau statistics

Catchments	**Catchment area (km^2)**	**Max. Kendall's tau value**		**No. of days prior to flood event**	
		MMPD events	**POT events**	**MMPD events**	**POT events**
Baronda	3,225	**0.90** [0.003]*	0.15 [0.41]	21	18
Ghatora	3,035	**0.90** [0.003]	**0.81** [0.01]	4	40
Kelo	950	0.36 [0.28]	**0.61** [0.02]	0	1
Kesinga	11,960	***0.80*** [0.08]	0.23 [0.28]	32	16
Kotni	6,990	0.05 [1]	0.16 [0.6]	34	30
Kurubhata	4,625	**1.00** [0.017]	**0.64** [0.03]	0	25
Manendragarh	1,100	0.24 [0.56]	***0.38*** [0.06]	40	27
Paramanpur	2,120	**0.71** [0.03]	0.47 [0.3]	26	38
Pathardhi	2,511	**0.62** [0.07]	0.42 [0.11]	12	4
Rajim	8,760	**0.62** [0.07]	0.21 [0.3]	3	29
Rampur	2,920	**0.90** [0.003]	0.51 [0.05]	4	4
Sundargarh	5,870	0.60 [0.23]	***0.31*** [0.08]	28	5

*the numbers in brackets indicates p-value for Kendall's τ correlation rounded up to two significant figures; higher (lower) value of Kendall's τ indicates stronger (weaker) correlation with a value of 1 (0) show perfect dependence (independence); p-value less than 0.05 and 0.10 indicate correlation value is statistically significant at 5 and 10% significant level and marked with bold and bold italics font respectively.

Table 2 Catchment-wise highest lagged *d*-day (varies from zero, the date of flood occurrence to 40 days prior to the event) correlation value of CW versus FT. The correlation values are computed using rank-based Kendall's tau statistics

Catchments	Catchment area (km^2)	Max. Kendall's tau value		No. of days prior to flood event	
		MMPD events	POT events	MMPD events	POT events
Baronda	3,225	***0.62*** [0.07]*	**0.71** [1.6e-5]	40	24
Ghatora	3,035	**0.88** [0.005]	**0.68** [0.04]	3	3
Kelo	950	**0.71** [0.01]	**0.72** [0.01]	40	29
Kesinga	11,960	**1.00** [0.02]	**0.74** [1.6e-5]	28	34
Kotni	6,990	**0.90** [0.003]	**0.73** [0.002]	40	40
Kurubhata	4,625	**1.00** [0.02]	**0.86** [0.002]	19	36
Manendragarh	1,100	**0.71** [0.03]	**0.64** [0.002]	36	25
Paramanpur	2,120	**0.71** [0.03]	***0.73*** [0.06]	40	35
Pathardhi	2,511	**0.71** [0.03]	**0.69** [0.005]	18	40
Rajim	8,760	**0.78** [0.02]	**0.67** [1.6e-5]	24	40
Rampur	2,920	**0.90** [0.002]	**0.78** [0.001]	40	40
Sundargarh	5,870	**1.00** [0.02]	**0.75** [1.6e-5]	20	35

*the numbers in brackets indicates p-value for Kendall's τ correlation rounded up to two significant figures; higher (lower) value of Kendall's τ indicates stronger (weaker) correlation with a value of 1 (0) show perfect dependence (independence); *p*-value less than 0.05 and 0.10 indicate correlation value is statistically significant at 5 and 10% significant level and marked with bold and bold italics font respectively.

List of figure captions

Fig. 1. **Study area map.** Elevation map and stream gauge stations (shown using red triangles) over the Mahanadi river basin. The index map shows the location of MRB (in green) in eastern India.

Fig. 2. **Temporal distribution of flood timing at MRB from 2007 to 2016.** (*left panel*) shows MMPD and the (*right panel*) shows POT events. The mean catchment elevations of stream gauges are expressed by the radius value. The flood timing is expressed by the angular position starting from 1 for the first day of the hydrological year (1st June). Since MRB is a rain-fed river most of the flood events are clustered between the beginning of the July and mid of the September month.

Fig. 3. **Temporal distribution of mean date and persistence of the 12 gauges.** (*left panel*) shows MMPD and (*right panel*) shows POT events. The size of the circle indicates the value of circular variance with larger (smaller) size indicates a larger (smaller) variance. The radii of the circular plots show the persistence in flood timing. The persistence measure close to 1 indicates floods tend to occur around the same day in the hydrological year.

Fig. 4. **Spatial map of persistence in flood timing.** (*Left panel*) shows the MMPD and (*right panel*) indicates POT events at individual stream gauge stations. The size and shade of the circle indicate the value of persistence measure with larger (smaller) size and darker (faded) shade show high (less) homogeneity in flood timing.

Fig. 5. **Correlation between catchment wetness (CW) and flood magnitude (FM).** Heat map showing rank-based Kendall's τ correlation between area weighted CW and FM for (*top panel*) MMPD and (*bottom panel*) POT events. Y-axis of the plots shows catchments arranged in an ascending order with respective to mean catchment elevation. The mean catchment elevations (in meters) are shown in brackets. The X-axis of the plot shows days, with d = 0 indicates the same day as the date of occurrence of the flood event; negative values indicate the days prior to flood event whereas positive value denotes the days after the flood event.

Fig. 6. **Correlation between catchment wetness (CW) and flood timing (FT).** Heat map showing rank-based Kendall's τ correlation between area weighted CW and FT for (*top*

panel) MMPD and (*bottom panel*) POT events. Y-axis of the plots shows catchments arranged in an ascending order with respective to mean catchment elevation. The mean catchment elevations (in meters) are shown in brackets. The X-axis of the plot shows days, with d = 0 indicates the same day as the date of occurrence of the flood event; negative values indicate the days prior to flood event whereas positive value denotes the days after the flood event.

Fig. 7. **Lagged *d*-day value of the maximum correlation between CW and FM.** *(left panel)* shows MMPD and *(right panel)* shows the POT events at individual stream gauge location. The size of boxes is proportional to the value of Kendall's τ with a larger box indicates high correlation whereas the smaller box shows a weaker correlation. The shade of the box indicates the lagged *d*-day value on which the maximum correlation was obtained, with lighter shade denotes the value of the *d-day* is close to the date of the flood event, while the darker shade indicates the value of the *d-day* is far from the date of the flood event.

Fig. 8. **Lagged *d*-day value of the maximum correlation between mean CW and FT.** (*Left panel*) shows the MMPD and (*right panel*) shows the POT events at individual stream gauge location. The size of boxes is proportional to the value of Kendall's τ with a larger box indicates high correlation whereas the smaller box shows a weaker correlation. The shade of the box indicates the lagged *d*-day value on which the maximum correlation was obtained, with lighter shade denotes the value of the *d-day* is close to the date of the flood event, while the darker shade indicates the value of the *d-day* is far from the date of the flood event.

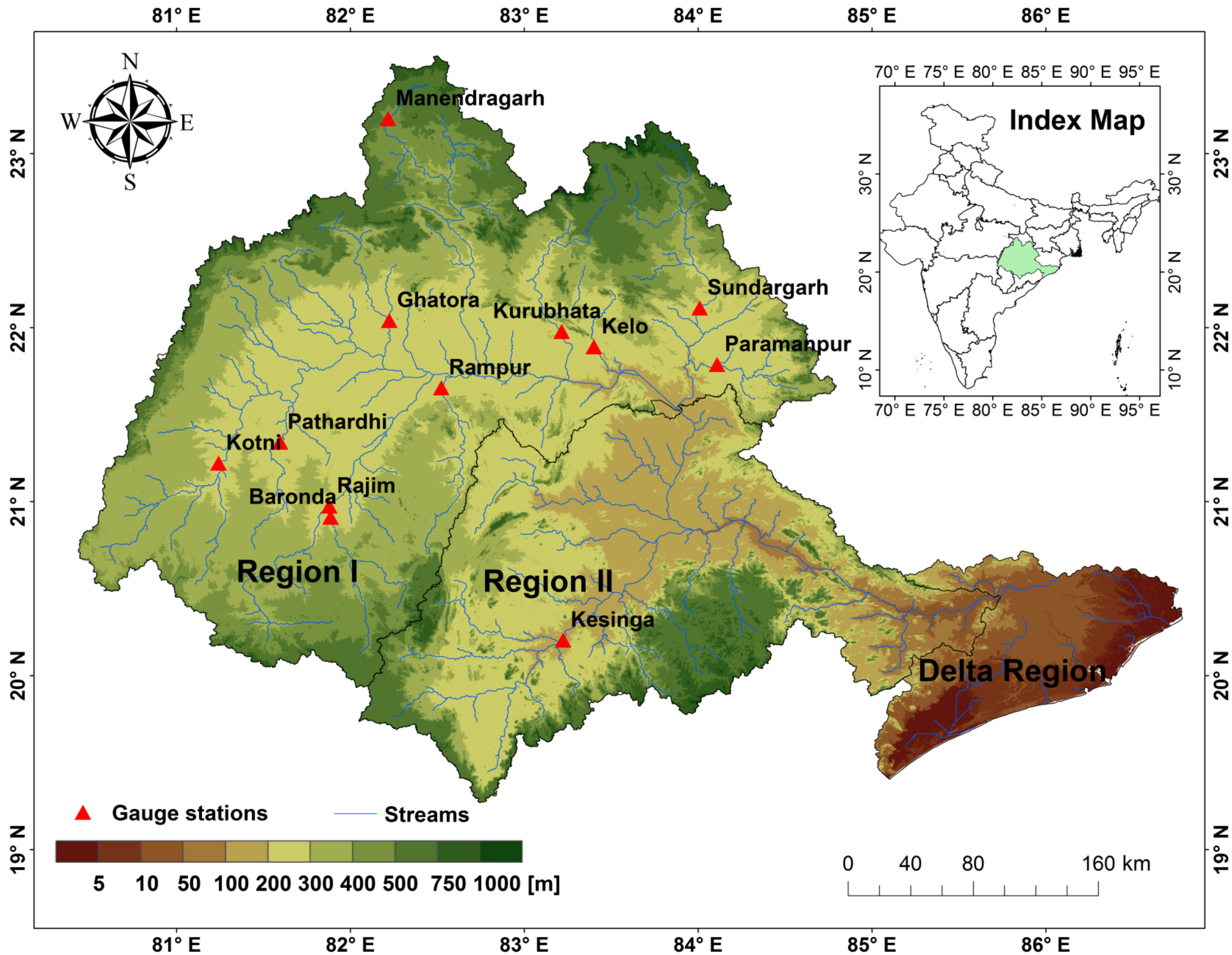

Fig. 1 Study area map. Elevation map and stream gauge stations (shown using red triangles) over the Mahanadi river basin. The index map shows the location of MRB (in green) in eastern India.

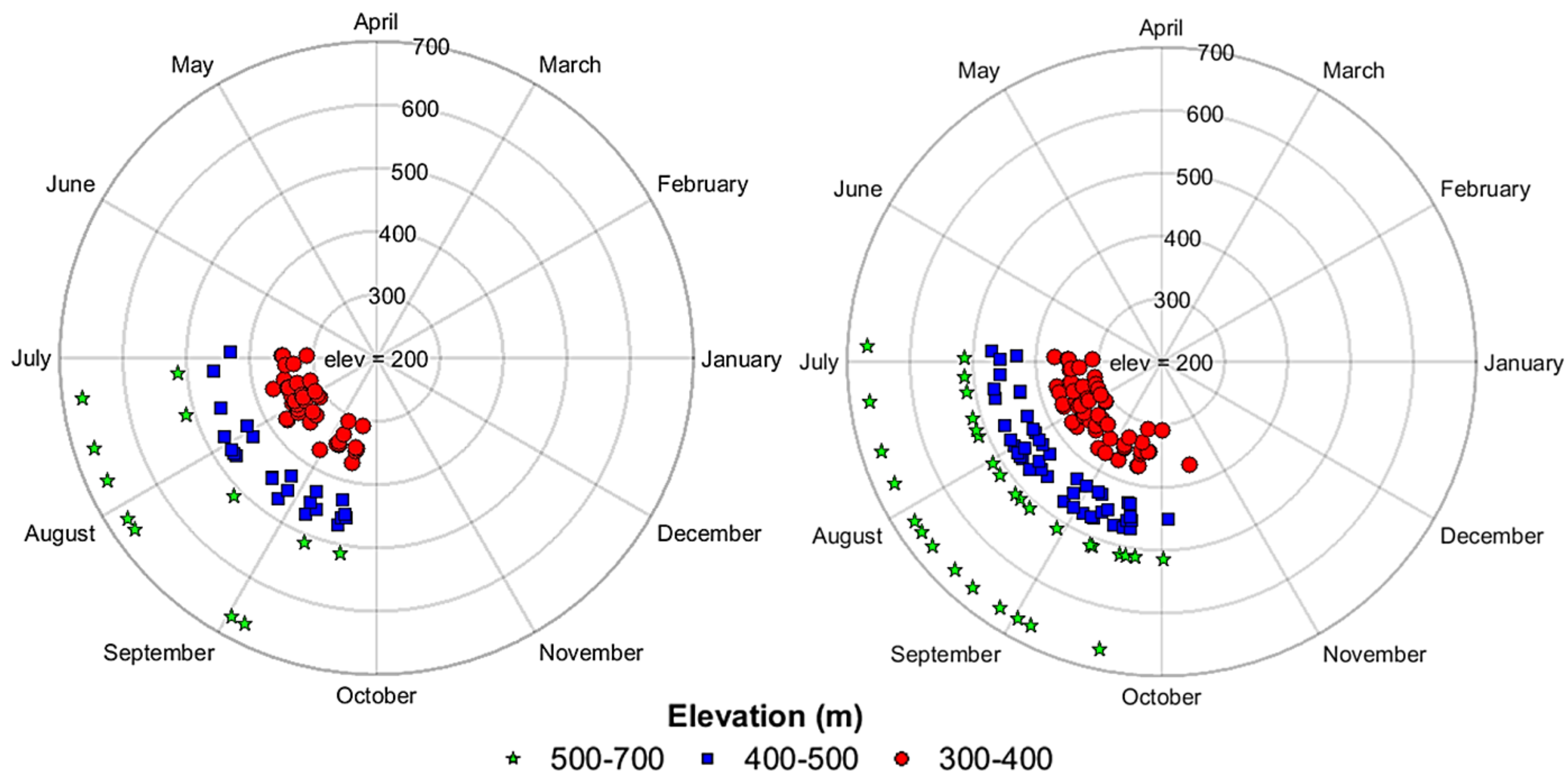

Fig. 2 Temporal distribution of flood timing at MRB from 2007 to 2016. (*left panel*) shows MMPD and the (*right panel*) shows POT events. The mean catchment elevations (in m) of stream gauges are expressed by the radius value. The flood timing is expressed by the angular position starting from 1 for the first day of the hydrological year (1st June). Since MRB is a rain-fed river most of the flood events are clustered between the beginning of the July and mid of the September month.

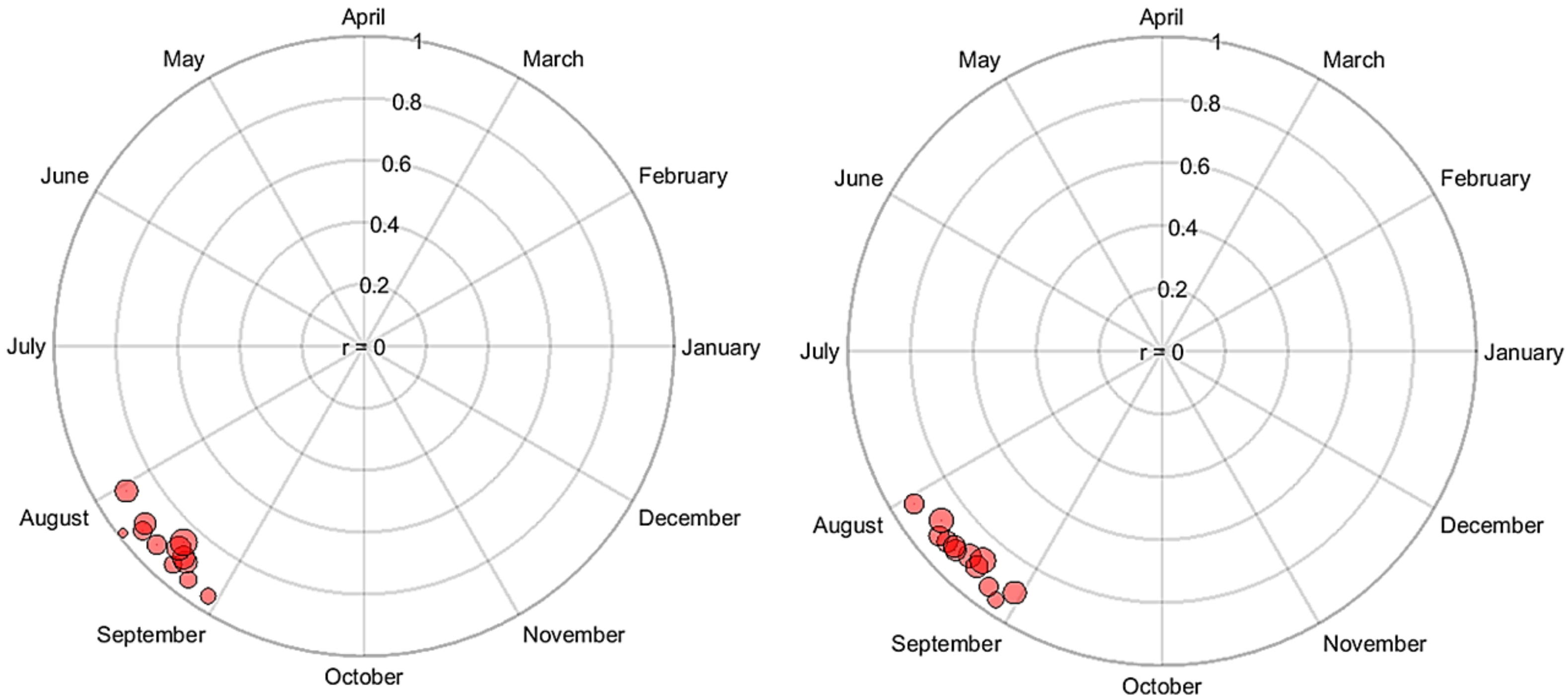

Fig. 3 Temporal distributions of mean date and persistence of the 12 gauges. (*left panel*) shows MMPD and (*right panel*) shows POT events. The size of the circle indicates the value of circular variance with larger (smaller) size indicates a larger (smaller) variance. The radii of the circular plots show the persistence in flood timing. The persistence measure close to 1 indicates floods tend to occur around the same day in the hydrological year.

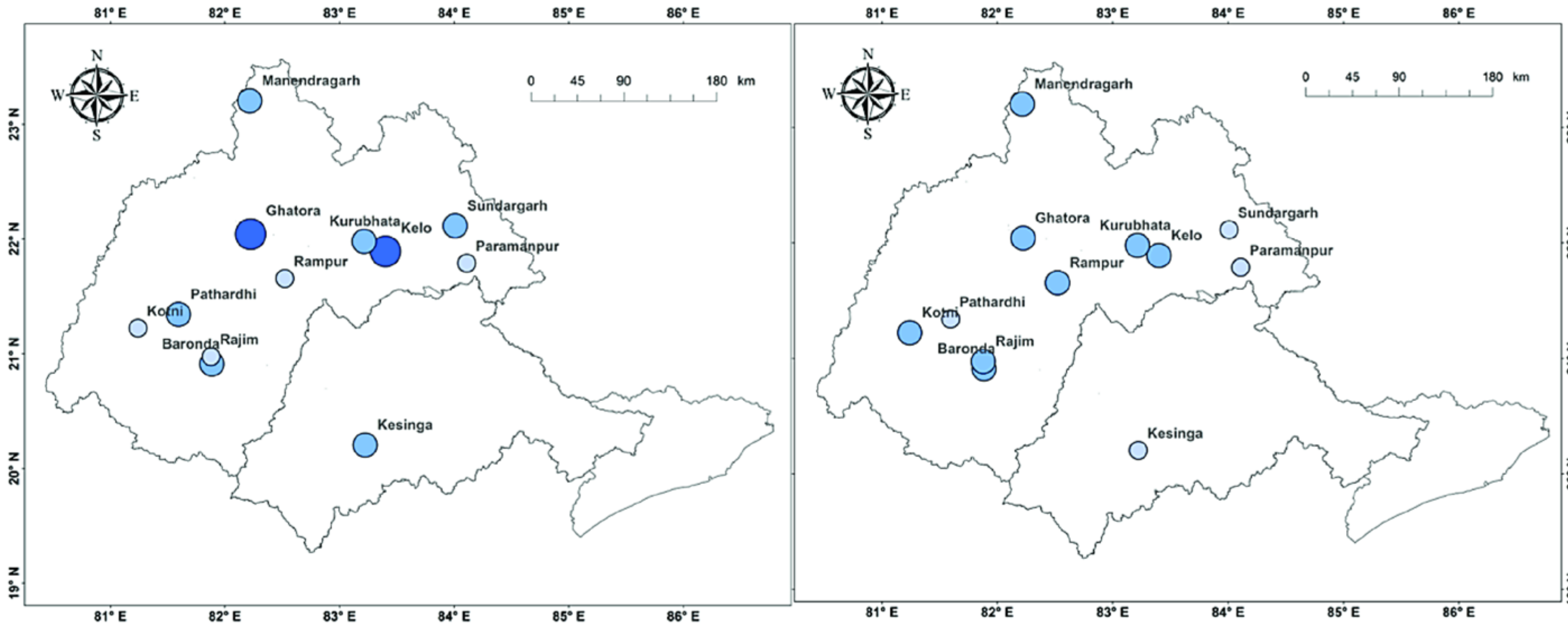

Fig. 4 Spatial distributions of persistence in flood timing. (*Left panel*) shows the MMPD and (*right panel*) indicates POT events at individual stream gauge stations. The size and shade of the circle indicate the value of persistence measure with larger (smaller) size and darker (faded) shade show high (less) homogeneity in flood timing.

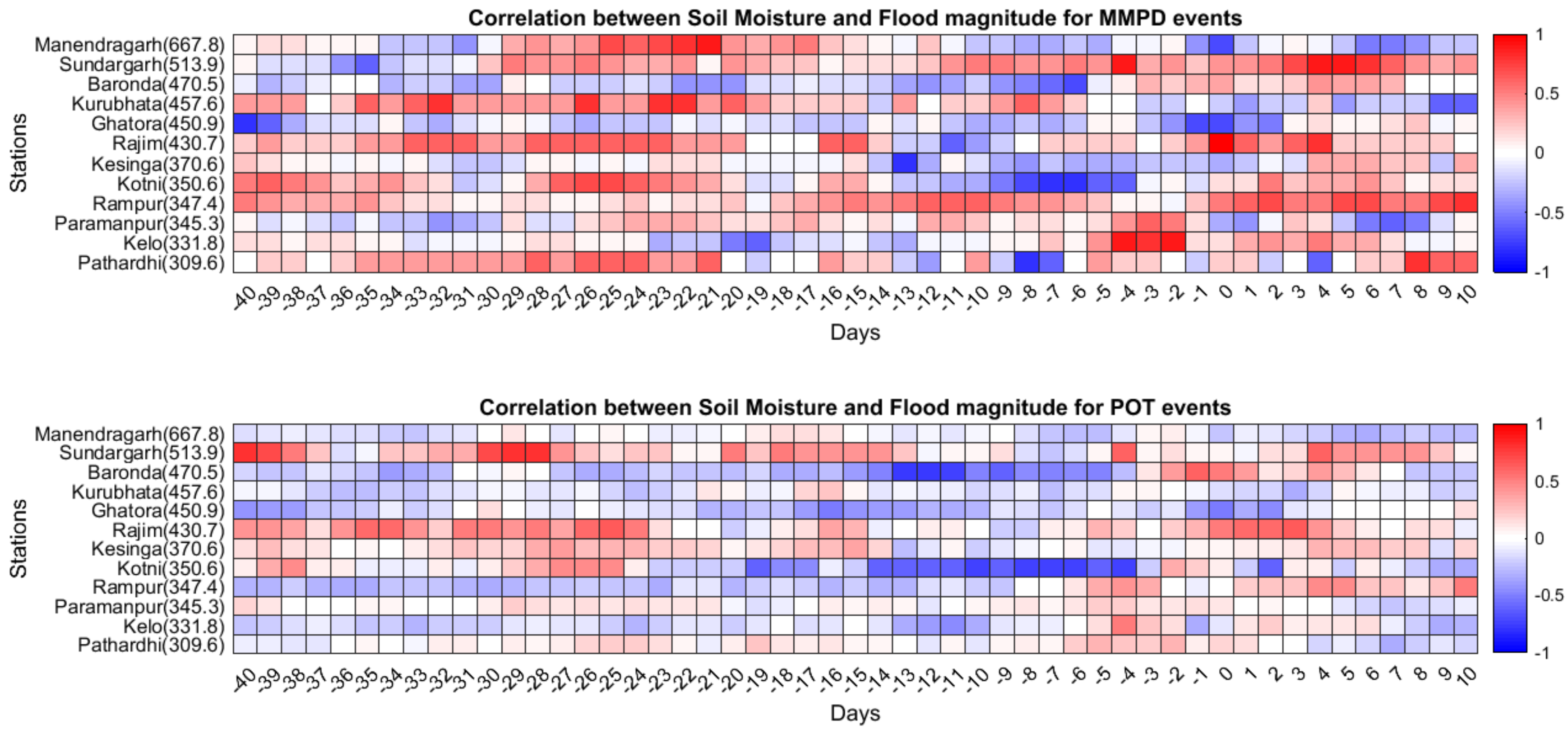

Fig. 5 Correlation between catchment wetness (CW) and flood magnitude (FM). Heat map showing rank-based Kendall's τ correlation between area weighted average CW and FM for (*top panel*) MMPD and (*bottom panel*) POT events. Y-axis of the plots shows catchments arranged in an ascending order with respective to mean catchment elevation. The mean catchment elevations (in meters) are shown in brackets. The X-axis of the plot shows days, with $d = 0$ indicates the same day as the date of occurrence of the flood event; negative values indicate the days prior to flood event whereas positive value denotes the days after the flood event.

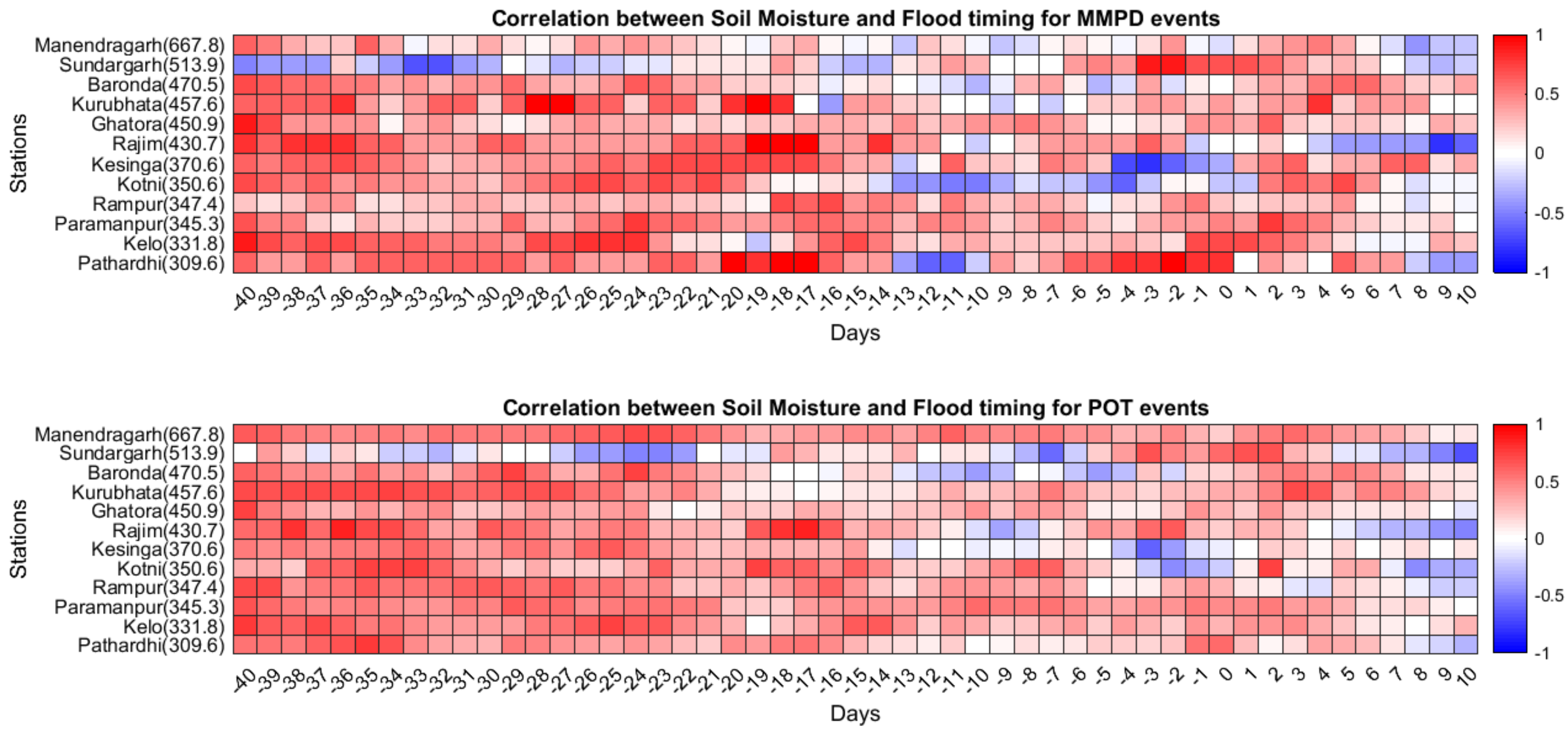

Fig. 6 Correlation between catchment wetness (CW) and flood timing (FT). Heat map showing rank-based Kendall's τ correlation between area weighted average CW and FT for (*top panel*) MMPD and (*bottom panel*) POT events. Y-axis of the plots shows catchments arranged in an ascending order with respective to mean catchment elevation. The mean catchment elevations (in meters) are shown in brackets. The X-axis of the plot shows days, with d = 0 indicates the same day as the date of occurrence of the flood event; negative values indicate the days prior to flood event whereas positive value denotes the days after the flood event.

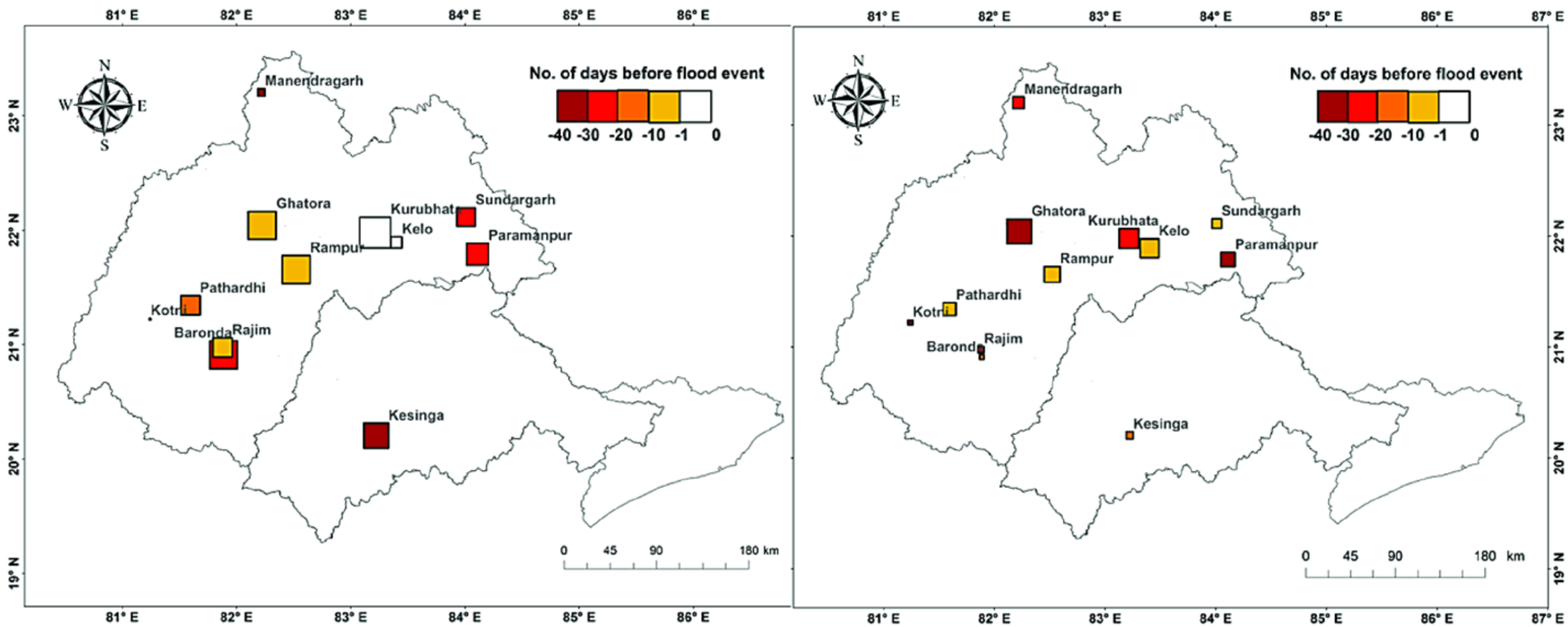

Fig. 7 Lagged *d*-day value of the maximum correlation between mean CW and FM. *(left panel)* shows MMPD and *(right panel)* shows the POT events at individual stream gauge location. The size of boxes is proportional to the value of Kendall's τ with a larger box indicates high correlation whereas the smaller box shows a weaker correlation. The shade of the box indicates the lagged *d*-day (*i.e.*, the number of days prior to flood event is shown using negative integer values) on which the maximum correlation was obtained, with lighter shade denotes the value of the *d-day* is close to the date of the flood event, while the darker shade indicates the value of the *d-day* is far from the date of the flood event.

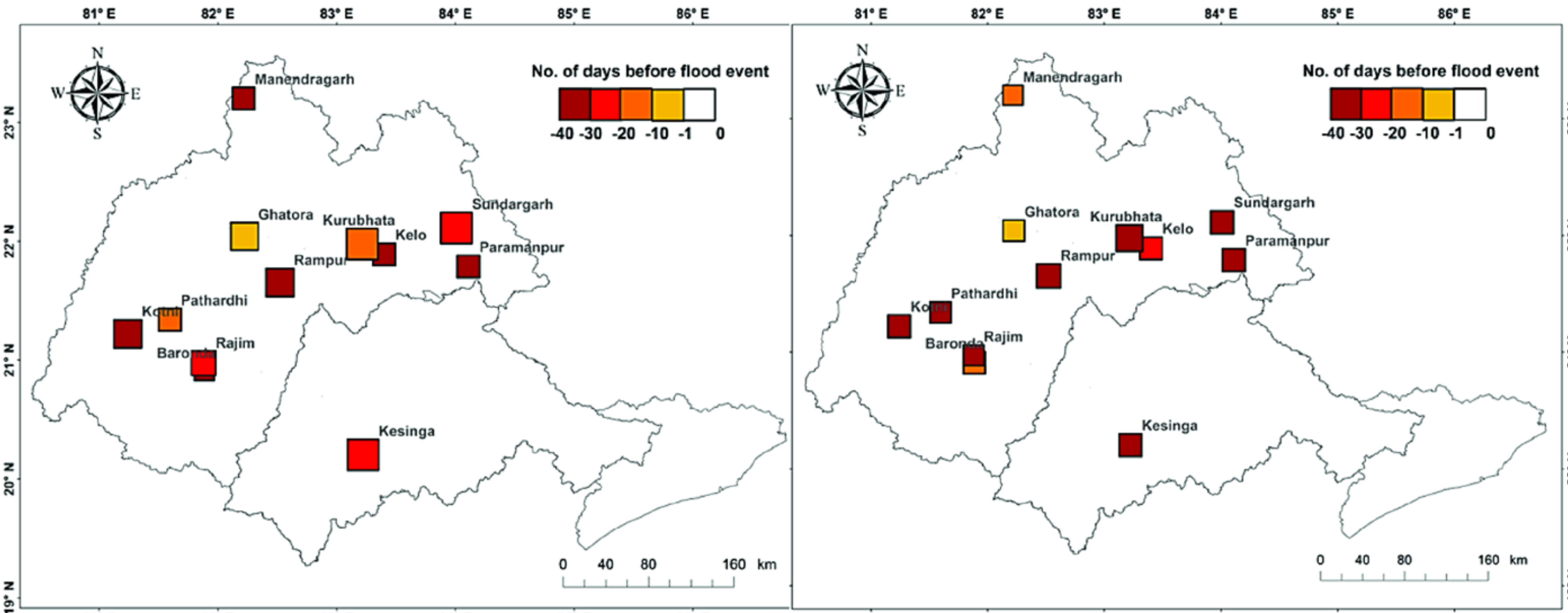

Fig. 8 Lagged *d*-day value of the maximum correlation between mean CW and FT. (*Left panel*) shows the MMPD and (*right panel*) shows the POT events at individual stream gauge location. The size of boxes is proportional to the value of Kendall's τ with a larger box indicates high correlation whereas the smaller box shows a weaker correlation. The shade of the box indicates the lagged *d*-day (*i.e.*, the number of days prior to flood event is shown using negative integer values) value on which the maximum correlation was obtained, with lighter shade denotes the value of the *d-day* is close to the date of the flood event, while the darker shade indicates the value of the *d-day* is far from the date of the flood event.